A methodological inter-comparison study on the detection of surface contaminant sodium dodecyl sulfate applying ambient- and vacuum-based techniques

A methodological inter-comparison study on the detection of surface contaminant sodium dodecyl sulfate applying ambient- and vaacuum-based techniques

Journal:	*Analytical and Bioanalytical Chemistry*
Manuscript ID	Draft
Type of Paper:	Research Paper
Date Submitted by the Author:	n/a
Complete List of Authors:	Giovannozzi, Andrea; INRIM, Hornemann, Andrea; Physikalisch-Technische Bundesanstalt, Cryophysics and Spectrometry Pollakowski, Beatrix; Physikalisch-Technische Bundesanstalt, Green, Felicia; National Physical Lab Gunning, Paul; Smith&Nephew Salter, Tara; University of Sussex Steven, Rory; National Physical Laboratory Bunch, Josephine; National Physical Laboratory, Portesi, Chiara; Istituto Nazionale di Ricerca Metrologica Tyler, Bonnie; Westfalische Wilhelms-Universitat Munster Physikalisches Institut Beckhoff, Burkhard; Physikalisch-Technische Bundesanstalt, X-ray Spectrometry group Rossi, Andrea M.; Istituto Nazionale di Ricerca Metrologica
Keywords:	sodium dodecyl sulfate, ambient mass spectrometry, Raman spectroscopy, Fourier-Transform infrared spectroscopy, reference-free X-ray fluorescence spectroscopy, biomedical devices

Cover letter Andrea Mario Giovannozzi

A. M. Giovannozzi
INRIM
Strada delle Cacce 91
10135 Torino, Italy

Torino, 01-August-18

Dear Editor, dear Referees,

Please find enclosed the manuscript entitled *"A methodological inter-comparison study on the detection of surface contaminant sodium dodecyl sulfate applying ambient- and vacuum-based techniques"* that I would like to present for your consideration for publication in *Analytical and Bioanalytical Chemistry.*

Our multi-technique approach focusses on the analytical research field of biomedical devices. Biomedical devices are complex products requiring numerous assembly steps along the industrial process chain carrying the potential of surface contamination. Cleanliness has to be analytically assessed with respect to ensuring safety and efficacy. Although several analytical techniques are routinely employed for process control, a reliable analysis chain with traceability is needed. This calls for multi-modal analytical methodologies that are cascaded in a sensible way to immediately identify and localize possible contamination, both qualitatively and quantitatively.

In this inter-comparative approach, we produced and characterized SDS model films that were deliberately deposited onto different flat in~/organic substrates, serving as potentially implementable reference materials for calibration ('model samples') of ambient techniques such as Ambient Mass Spectrometry (AMS), Infrared and Raman spectroscopy.
Moreover, 'real samples', i.e. biomedical devices with a convex geometry, such as a hip liner, were deliberately contaminated with SDS in order to emulate a contaminated sample emerging from an industrial process chain.
We demonstrate that non-invasive and complementary Raman and IR spectroscopy offer *a priori* chemical identification with integrated chemical imaging tools for qualitatively and quickly following the contaminant distribution on the µm scale, even on hip liner devices. Both readout techniques may be slotted in ahead all other remaining techniques discussed in our inter-comparison approach, followed by the traceable reference-free XRF analysis.

AMS capable to provide mass spectroscopic fingerprints for fast qualitative identification of surface contaminations we consider to be used at the end of the traceability chain, as it is moderately destructive technique relying on the removal of material from the sample surface.

To absolutely determine the mass deposition of SDS, vacuum-based reference-free XRF was implemented. Since ambient techniques necessitate reference materials / standards for quantitative analyses, SI-traceable XRF was capable to quantify the amount of organic SDS contaminant on in~/organic substrates.

Summarizing all, our approach demonstrates that the increase of information depth provided by combining all techniques has the potential to enable even on-line characterization and chemical speciation within the process chain in the biomedical device industry

We believe in the novelty of our multi-modal approach undertaken in this manuscript as an easily implementable high-throughput readout platform of high relevance in the field of biomedical device industries. We think that our findings could appeal to a broad, multi-disciplinary readership of *Analytical and Bioanalytical Chemistry*.

Yours Sincerely,

A. M. Giovannozzi and on behalf of all co-authors

A methodological inter-comparison study on the detection of surface contaminant sodium dodecyl sulfate applying ambient- and vacuum-based techniques

Andrea M. Giovannozzi[a,*], Andrea Hornemann[b], Beatrix Pollakowski-Herrmann[b], Felicia M. Green[c], Paul Gunning[d], Tara L. Salter[c,e], Rory T. Steven[c], Josephine Bunch[c,f], Chiara Portesi[a], Bonnie J. Tyler[g], Burkhard Beckhoff[b], and Andrea Mario Rossi[a]

[a]*Quality of Life Division, INRIM, Strada delle Cacce 91, 10135 Torino, Italy*
[b]*Physikalisch-Technische Bundesanstalt Berlin (PTB), Abbestr. 2-12, 10587 Berlin, Germany*
[c]*National Centre of Excellence in Mass Spectrometry Imaging (NiCE-MSI), National Physical Laboratory, TW11 0LW, United Kingdom*
[d]*Smith & Nephew Advanced Wound Management, 101 Hessle Road, Hull HU3 2BN, United Kingdom*
[e]*Department of Chemistry, School of Life Sciences, University of Sussex, Falmer, Brighton, BN1 9QJ, UK*
[f]*Department of Surgery & Cancer, Computational and Systems Medicine, Imperial College London, SW7 2AZ, UK*
[g]*University of Münster, 48149 Münster, Germany*

[*]*Corresponding author:*
Dr. Andrea M. Giovannozzi,
tel +39 011 3919330
fax +39 011 346384
e-mail a.giovannozzi@inrim.it

Electronic Supplementary Material (ESM) available.

Abstract

Biomedical devices are complex products requiring numerous assembly steps along the industrial process chain, which can carry the potential of surface contamination. Cleanliness has to be analytically assessed with respect to ensuring safety and efficacy. Although several analytical techniques are routinely employed for such evaluation, a reliable analysis chain that guarantees metrological traceability and quantification capability is desirable. This calls for analytical tools that are cascaded in a sensible way to immediately identify and localize possible contamination, both qualitatively and quantitatively.

In this systematic inter-comparative approach, we produced and characterized sodium dodecyl sulfate (SDS) films mimicking contamination on inorganic and organic substrates, with potential use as reference materials for ambient techniques, i.e., Ambient mass spectrometry (AMS), Infrared and Raman spectroscopy, to reliably determine amounts of contamination. Non-invasive and complementary vibrational spectroscopy techniques offer *a priori* chemical identification with integrated chemical imaging tools to follow the contaminant distribution, even on devices with complex geometry. AMS also provides fingerprint outputs for a fast qualitative identification of surface contaminations to be used at the end of the traceability chain due to its ablative effect on the sample. To absolutely determine the mass of SDS, the vacuum-based reference-free technique X-ray fluorescence was employed for calibration. Convex hip liners were deliberately contaminated with SDS to emulate real biomedical devices with an industrially relevant substance. Implementation of the aforementioned analytical techniques is discussed with respect to combining multimodal technical setups to decrease uncertainties that may arise if a single technique approach is adopted.

Keywords

sodium dodecyl sulfate, ambient mass spectrometry, Raman spectroscopy, Fourier-Transform infrared spectroscopy, reference-free X-ray fluorescence spectroscopy, biomedical devices

Introduction

Biomedical devices such as implantable joint prostheses, orthopedic pins, plates, nails and cardiovascular stents are complex products requiring significant manufacturing and assembly steps. This may give rise to surface contamination from process fluids, lubricants, cleaning fluids or other residues, which has to be removed and rinsed away prior to final packaging of the product. Many materials such as detergents, surfactants and buffers are often employed for cleaning, but their intensive use has to be carefully evaluated in order to avoid the introduction of new residues or their solubilization and migration from one location to another. Moreover, the effectiveness of the cleaning process has to be considered with respect to the potential damage of the device since these chemicals are often used in combination with mechanical and thermal treatments. Therefore, the entire approach for assessing the cleanliness of a medical device has to be analytically evaluated for ensuring both safety and efficacy of the product.

Manufacturers strive for the highest quality final products whilst also desiring improvements in manufacturing efficiency by using cost-effective, industrially practical high-throughput analysis technologies. Various analytical methods are used to evaluate the cleanliness of biomedical devices such as Gas chromatography–Mass Spectrometry (GC-MS), High pressure Liquid chromatography–Mass Spectrometry (HPLC-MS), Inductively coupled plasma-Mass Spectrometry (ICP-MS), X-ray diffraction (XRD) and Gravimetric analysis

[1,2], which usually guarantee high sensitivity in the quantification of the contaminants upon extraction and separation steps. However, they cannot provide information about the spatial distribution of any contaminants, whose knowledge is fundamental to provide clues as to the how/where in the manufacturing and cleaning history the contamination has occurred and how different surface finishes or materials may be more or less susceptible to contamination.

High-end surface analytical methods such as X-ray photoelectron spectroscopy (XPS) or Time-of-Flight Secondary Ion Mass Spectrometry (ToF-SIMS) are ideally suited spectroscopic techniques that can provide both high sensitivity and spatially resolved information with high surface specificity. However, these methods are both time-consuming, mainly owing to the need for high vacuum and for appropriate (potentially time consuming) sample preparation and significant expense. They are also generally incapable of handling the complex geometry of complete medical devices. Hence, there is a need for analytical methods that provide trace-level sensitivity and surface selectivity and specificity, whilst providing spatially resolved information, preferably with the option to deploy such methods at point of manufacture or distribution. The latter requirement implies a high degree of convenience and rapid throughput practicality. Emerging ambient techniques, either based on vibrational spectroscopy or mass spectrometry, for instance, are far better suited to the manufacturing environment, but currently these techniques lack reproducibility and traceability, as they rely on standards / reference materials needed for the characterization of advanced biomaterials and complex sample presentation requirements to enable quantitation.

The aim of our work is to develop the foundation metrology needed to provide robust, reproducible, surface sensitive and selective analysis of biomedical device materials by using Ambient Mass Spectrometry (AMS), Fourier-Transform infrared (FTIR) microscopy and Micro-Raman Spectroscopy. AMS-based techniques such as Desorption Electrospray

Ionization (DESI), Plasma Assisted Desorption Ionization (PADI) and Liquid Extraction Surface Analysis (LESA) already demonstrated their applications as indispensable tools for polymer science [3], pharmaceutical science [4], and biosamples (biofluids, tissues, cells) characterization combined with imaging tools [5,6]. AMS has been, as far as we are aware, rarely used, in relation to surface contaminants analysis on real biomedical devices and specifically for characterization of typical surface contaminants [7]. Similarly to vibrational spectroscopies, AMS can provide rich chemical information, highly specific for polymers or even impurities on mixed polymeric materials, enabling quantitative structural analytics. Micro-FTIR and micro-Raman spectroscopy also offer great promise for meeting the medical device industry needs for on-line surface quality assessment and process control [8]. In addition to providing detailed and specific chemical information by FTIR/Raman-based molecular fingerprints, both techniques enable non-destructive readout, and can be combined with a micro-spectroscopic setup. Such chemical imaging can provide insights into contaminant distribution on devices and by providing semi-quantitative spatially resolved information.

Herein we present a systematic study on a commonly encountered small molecule detergent, namely sodium dodecyl sulphate (SDS), that is widely manufactured and used in household detergents, personal care products, emulsification, lubrication, catalysis, plastics industry, and electroplating [9–11]. A variety of surfactants, including the anionic type employed in this study, show relatively low biodegradability and a high tendency to be absorbed by natural materials [12]. Consequently, they are harmful to humans and carrying bacteria and pollutants over quite a long distance [13]. Several approaches were developed to detect SDS, mostly based on spectrophotometric, amperometric, fluorescence, chromatographic and biosensing analysis [14–19]. However, these techniques have low specificity, as they cannot distinguish

similar but different surfactants. They can be applied restrictively, as they usually enable the analysis of liquids, thus hindering their use for *in situ* detection.

This calls for new strategies for setting up robust and combined analytical methods for sensitive, selective, and early-stage characterization of surfactants within the industrial processing chains.

We investigated the SDS physicochemical distribution and amount on different sample substrates, based on inorganic (silicon: Si, and stainless steel: SST) and organic materials (high-density polyethylene: HDPE), utilizing ambient techniques such as AMS, FTIR, and Raman micro-spectroscopy, and vacuum-based techniques such as X-ray fluorescence spectroscopy (XRF). While ambient techniques necessitate reference materials / standards for quantitative analyses, XRF analysis is capable of absolute quantitative determination of the content of in~/organic components, enabling a reference-free SI-traceable quantification of the contaminant on the surface [7]. This inter-comparison study provides spatially resolved information related to the specificity and sensitivity of SDS detection, with regard to the use of both ambient and vacuum techniques.

Moreover, real biomedical devices with a complex geometry such as a hip liner were deliberately contaminated with SDS in order to emulate a real contaminated sample system from an industrial processing chain, and were analyzed by means of all analytical techniques to test their efficiency of detection.

Materials and Methods

Chemical reagents

Sodium dodecyl sulfate (Sigma Aldrich, MW: 288.38 g/mol, > 99.0 % purity) and formic acid (99%, Sigma-Aldrich) were purchased from Sigma Aldrich. The solvents used were deionized

water (>18 MΩ cm^{-1}), acetonitrile (ACN) (99.99 Sigma, UK), methanol (MeOH), ethanol (EtOH) and propan-2-ol (IPA) (FisherScientific, UK).

SDS was deposited onto substrates of Silicon (Si), Stainless Steel (SST) and High Density Polyethylene (HDPE). Stainless Steel was supplied by Goodfellow AISI 316 (Fe/Cr18/Ni10/Mo3) Foil, 0.914 mm thick annealed. Upon arrival of the SST, one face was polished to a high shine. HDPE wafers were supplied from Sigma Aldrich and modified using a heat press to ensure a flat surface.

Preparation of SDS model contaminant films on Si, SST and HDPE substrates

For the preparation of the model systems used in the comparative study, SDS was deposited onto clean Si, SST and HDPE substrates with a TM sprayer (HTX Technologies). The SDS spraying condition was as follows: flow rate 0.125 mL/min, gas pressure 10 psi, spraying temperature 80 °C, velocity 1333 mm/min, number of passages 8, track spacing 3 mm with an offset spacing of 1.5 mm. SDS was dissolved in 80% methanol solution at 0.25 mg/mL concentration and spray-coated onto the sample substrates to a surface concentration of 5×10^{-6} g/cm^2 which, with an assumed density of 1.01 g/cm^3 for SDS, equates to a layer thickness of approximately 50 nm. Solution concentrations of 0.25 mg/mL were chosen as being close to the critical micelle concentration (CMC) of SDS, which ranges between 0.17 and 0.23 % w/v (in water/buffer). SDS has been demonstrated to inhibit mammalian cell culture at concentrations close to its CMC [20].

Contamination of hip liners with SDS as 'real samples'

Hip liners from Smith & Nephew were deliberately contaminated with SDS in order to emulate real biomedical devices with a low enough level of contamination to be analytically

challenging yet illustrative of whether such low level contamination in an industrial processing chain may be detectable on a real product surface. The hip liner consisting of ultra-high-molecular-weight polyethylene (UHMWPE) was contaminated with SDS using an airbrush. A solution of 0.25 mg/mL was sprayed as homogeneously as possible to produce a film thickness of ~50 nm.

Vacuum-based techniques

XRF analysis

For the quantitative analysis of SDS, the Plane Grating Monochromator (PGM) beamline for undulator radiation at the PTB laboratory at BESSY II was employed [21–23]. The beamline PGM-U49 provides monochromatized undulator radiation in the energy range from 78 eV to 1870 eV with high spectral purity and well-known flux (or radiant power) [21,22]. Attached to this beamline, an ultra-high vacuum chamber has been used, equipped with a 9 axis manipulator, enabling a very precise adjustment of the samples, and in particular, extremely precise control of incidence angle [24]. This UHV chamber and the sample holder is placed in the focal plane of the PGM beamline, which has a vertical size of about 170 µm. The excited fluorescence radiation is detected by a radiometrically calibrated energy-dispersive Silicon drift detector (SDD) [22]. Calibrated means in that sense, that the efficiency and the detector response functions are well-known. In addition, the solid angle of detection can be determined as described in ref. [25]. For a more precise determination of the solid angle of detection, a calibrated diaphragm was used. In case of the coated hip liners, it has been employed due to the fact that the incidence angle is not well-defined because of the irregular curved surface of the hip liner, having a significant impact on quantification. For the model systems, this was not the case, so the determination was carried out as described in ref. [25]. The radiant power

or flux from the beamline is detected by calibrated photo diodes with known response for photon energy. All these calibrated instruments allow for a reference-free quantification of the mass per unit area and the elemental composition by employing a fundamental parameter approach [25].

Reference-free XRF

The quantitative analysis of the absolute mass per unit area and the elemental composition was carried out by using a fundamental parameter approach as introduced by Beckhoff *et al*. [25]. Here, all experimental and atomic fundamental parameters have to be well-known. For this purpose, the calibrated instrumentation described in the ESM is used.

For the reference-free quantification of SDS, X-ray fluorescence analysis under grazing incidence conditions and in conventional 45° / 45° geometry was carried out. The model systems were measured at an incidence angle of about 45° and at a photon energy of 1622 eV. Here, the Na Kα, O Kα, and C Kα fluorescence line intensities were used for the quantification. The hip liners were analyzed by using a photon energy of about 1487 eV to excite all the relevant elements excluding sulfur. The incidence angle was approximately 10°.

Ambient Techniques

Ambient Mass Spectrometry – PADI, DESI and LESA MS

Different atmospheric pressure desorption/ionization sources were used: a plasma assisted desorption ionization (PADI) source [26], a Prosolia 2D automated Omni Spray Ion Source (Indianapolis, USA) for desorption electrospray ionization (DESI) source [27] and an Advion Biosciences TriVersaNanoMatesource (Harlow, UK) for liquid extraction surface analysis (LESA) measurements [28]. These were coupled to a Thermo Scientific LTQ-OrbitrapVelos

mass spectrometer, and experiments were performed using the high mass resolution setting of 100,000 at m/z 400.

DESI was set up as optimized; briefly, a solvent flow rate of 2 µL/min was used. The voltage was 5 kV and nitrogen gas was supplied at 100 psi. The electrospray was freshly prepared, either using 50% methanol or 90% acetonitrile with 0.01% formic acid in deionized water. The PADI instrument was built in-house at the National Physical Laboratory, UK and the set up was optimized as described in ref. [29]. A plasma power of 15 W and helium flow rate of 800 ml/min was used. The LESA technique parameters used in this investigation were as follows: solvent volume 3 µL, solvent depth 1 µL, dispense 2 µL, delay 2 s, aspirate 1.8 µL, dispensing height -7.0 mm, aspiration height -7.0 mm, delivery time 1 min, gass pressure 0.3 psi, and voltage 1400 V.

Synchrotron radiation (SR)-based FTIR spectroscopy

FTIR spectroscopic measurements were performed at the IR beamline 'IRMA' of the electron storage ring Metrology Light Source (MLS) of PTB which is optimized for the wavelength range between 1 µm and 20 µm [30,31]. Experiments were performed with a Vertex-80v FTIR spectrometer coupled to an IR microscope Hyperion 3000 (Bruker Optics GmbH, Germany) equipped with a 128^2 pixels FPA detector (Focal Plane Array, pixel size ~ 3 µm at 15× magnification) and Mercury Cadmium Telluride (MCT) detector. For point-wise FTIR spectroscopical measurements, the SR source (σ_x=670 µm, σ_y=183 µm, beam current ~170 mA) was focused through an ATR (attenuated total reflection) objective of 15 fold magnification onto the model sample systems; here SDS-coated Si, SST and HDPE substrates were investigated. Additionally, the HDPE-based Hip Liners with/without SDS contamination as "real sample systems" were analyzed by FTIR-ATR spectroscopy. MIR-spectra from 3900

cm^{-1} to 900 cm^{-1} were acquired with the MCT detector system in reflection mode by co-adding 128 scans at 4 cm^{-1} resolution for the data acquisition. Background scans were collected before each sample measurement from a region free of sample and a ratio was taken against the sample spectrum.

Raman micro-spectroscopic analysis

Raman spectra were recorded using a dispersive Thermo Scientific DXR Raman spectrometer equipped with a microscope, an excitation laser source at 455 nm or 532 nm, a motorized stage sample holder (step size: 1 µm), and a charge-coupled device (CCD) detector. Spectra of SDS model systems on Si, SST and HDPE were collected using a 100× microscope objective (laser spot diameter: 0.6 µm) with a laser power from 5 mW to 10 mW and a spectral range from 3500 cm^{-1} to 50 cm^{-1} with a grating resolution of 5 cm^{-1}. The acquisition time was of 100 scans with 5 s exposure time. Same parameters were used for the analysis of the UHMWPE - based hip liners contaminated with SDS.

Micro-Raman Imaging Spectroscopy of SDS model systems was conducted with a DXR™ xi Raman Imaging Microscope (Thermo Scientific) using a laser wavelength at 455 nm, a laser power of 5 mW, a 50× microscope objective and a motorized stage with a 2 µm step size. Spectra were collected in the 3500 cm^{-1} - 50 cm^{-1} spectral region with a grating resolution of 5 cm^{-1}, an exposure time of 0.02 s and 100 scans in total. Raman chemical images were represented using a false color scale, from blue (low signal) to red (high signal), related to the intensity of the symmetric stretching of the SO_4 at 1083 cm^{-1}.

Results & Discussion

XRF analysis on SDS model contaminant layers

In order to develop and evaluate consistent SDS model layers systems that should function as potential reference/calibration samples, investigations on homogeneous integrity and contamination thicknesses of the respective sprayed SDS layers were firstly performed by XRF. Specifically, SDS contaminants' layer thicknesses were absolutely determined by non-destructive reference-free XRF and their distribution on each type of substrate was evaluated on the basis of the XRF signal response obtained at different sample positions.

The model systems were measured at an incidence angle of about 45° at a photon energy 1622 eV (Table 1). Here, Na Kα, O Kα, and C Kα fluorescence line intensities were used for the quantification.

Fig.1

In Fig. 1 typical XRF spectra are shown for different types of substrate samples which are characterized by the fluorescence lines of the SDS (C, O, and Na) and the respective substrate material, as Cr, Fe, and Ni for the stainless steel substrate, and Si for the wafer. For the quantification of SDS, the intensity of the fluorescence lines of sodium was analyzed. The elements carbon and oxygen were only used for comparison, because the substrate material contains significant fractions of them. Assuming the Na mass deposition arises only from the SDS and the stoichiometry of SDS is known, the mass deposition of all other involved elements was determined.

Table 1

If knowledge of the density is available, the mass deposition can be converted into thickness. Here, the thickness is determined assuming the bulk density of SDS. The thickness of SDS is about 44 ± 6 nm for the SST substrate, 41 ± 6 nm for HDPE and 37 ± 6 nm for the Si wafer. From the deposition process of the SDS layer, the nominal thickness was assumed to be about 50 nm. The experimentally determined thicknesses are in the same order of magnitude, but slightly thinner, in particular for the deposition on Si.

Considering the mass deposition of oxygen, the determined content includes additional contributions from the substrates excluding the HDPE, which has only minor surface contamination. The Si substrate shows the smallest amount of adventitious C contaminations. Further, this methodology turned out to be very suitable for extracting information of elemental composition, not only from the surface contaminant layers, but also from the bulk material, providing overall information on impurities and on potential qualification as a reference sample system.

Ambient Mass spectrometry – PADI, DESI and LESA

The model SDS systems were used to assess the ability of different AMS modalities, PADI, DESI and LESA, for the detection of SDS from different bulk substrate surfaces. AMS addresses the need for rapid analysis with minimal sample preparation. It is known that AMS can potentially provide semi-quantitative information required for assessing the average molecular mass distribution of polymers [32]. Furthermore, molecule ion spectra deliver a characteristic fingerprint-like pattern through which distinct identification of the polymer's composition and polymerization state is possible. The latter measurand allows acquisition of information related to the amount of polymeric impurity residues emerging during industrial

manufacturing [33]. Additionally, examples of in-line use of AMS can be found in, crop science, biomedical and surgical scenarios [34,35], thus evidencing their potential utility in automated manufacturing settings. In the following, diverse AMS sampling techniques were applied and compared with respect to their signal outputs related to SDS contaminant detection. Plasma ionization MS has previously been demonstrated to successfully ionize a variety of molecular classes in the context of PADI MS [36] as well as when serving as a post ionization mechanism in laser desorption MS [37]. However, it is also understood that despite encouraging reports in assisting ionization plasma devices can perform poorly as desorption devices, particularly where the analyte of interest is non-volatile or present on the surface in a physical form not conducive to PADI analysis [38]. Consequently, it was determined in preliminary studies (data not shown) that PADI was not a suitable desorption ionization technique for analysis of SDS samples of the form studied here and those likely to be encountered medical device contamination studies. DESI and LESA MS were able to successfully detect the molecular SDS ion from 50 nm thick films, either on Si, SST and HDPE substrates.

Fig.2

SDS was primarily detected in negative ion mode with the loss of the sodium cation [M-Na]- ($C_{12}H_{25}O_4S$) at m/z 265.147 (singly charged mon-isotopic mass with sodium loss). Example mass spectra are shown in Figure 2a and b for DESI and LESA respectively. The peak signal intensities of the molecular ions vary according to the substrate and solvent used in DESI, probably due to the differences in wettability and conductivity of the different substrate surfaces (see Table S-2, ESM for details). This needs to be taken into consideration when comparing data qualitatively from different samples. LESA analysis also demonstrated successful detection of the 50 nm SDS films on PE, Si and SST substrates in the negative ion

mode, although any substrate related effects were unclear. It is shown that LESA also successfully detects the molecular anion as with DESI.

In summary, the variation of intensity observed for SDS contamination is closely related to the difference in the AMS-based sampling technique that was implemented here, either by using DESI and LESA. These preliminary results therefore demonstrate the potential utility of both LESA and DESI mass spectrometry for use in-line with manufacturing processes. Testing on real world sample forms is a critical next step and will be addressed below.

FTIR and Raman micro-spectroscopic analyses

Vibrational spectroscopy was conducted by exploiting the mutually complementary character of both FTIR and Raman fingerprinting techniques in order to assess a full picture of the SDS molecular composition on the different types of substrates. In Fig. 3a-b FTIR and Raman spectra recorded on the different model systems, i.e. SDS on Si, SST and HDPE, together with the reference fingerprint of the SDS obtained from the pure powder, are shown.

Fig.3

The main vibrational features of the SDS molecule are visible in the stretching region of the CH_x groups at 3000-2800 cm^{-1} attributed to the symmetric and anti-symmetric CH_2/CH_3 stretching modes, in the region between 1500 cm^{-1} and 1050 cm^{-1} which contains the C-C skeletal vibrational modes (between 1050 cm^{-1} and 1150 cm^{-1}) and the CH_2 bending modes (1440-1460 cm^{-1}), and in the alkyl sulfonate region attributed to the SO_4/SO_3 groups that occurs between 1300-1000 cm^{-1} and 1000-400 cm^{-1} for FTIR and Raman, respectively. The tentative IR and Raman assignments attributed to the SDS thin film can be found in more detail in Table S-3 (ESM). Interestingly, as the comparison of the relative ratios of the SDS modes in the FTIR and Raman spectra show, the symmetric bonds, such as the CH_x and C-C

skeletal vibrational modes, are stronger in the Raman spectra, while the asymmetric and polar bonds, such as the ones related to the SO_4, are more dominant in the FTIR spectra (Fig.3a-b). This behavior is consistent with the nature of the molecular transitions that take place in these two techniques, highlighting the importance of a complementary characterization to provide useful information on the analyzed substrate and on the efficient detection of the SDS.

FTIR experiments in ATR configuration turned out to be very suitable for the sensitive detection of SDS thin layer coatings on all SDS-coated substrates in the 50 nm regime, likewise by taking advantage of the polarized synchrotron radiation that was guided through the ATR crystal sample interface to enable an effective enhancement of the SDS signal. No assignable overlaps can be found with the sample substrate spectra, apart from the HDPE sample substrate, the SDS samples were ratioed against their corresponding backgrounds (Si and SST). For the SDS on HDPE we took a low-emissivity reflective substrate (Kevley Technologies Inc.), as it provides featureless detection in this spectral region of interest and enables an adequate instrumental function and atmospheric background correction. Consequently, we can also observe spectral contributions from HDPE [39], but they do not strongly interfere (except for the CH_2 deformation mode at ~1470 cm^{-1} and CH_2 stretching vibration at ~2915 cm^{-1}) with the SDS modes (Fig. 3a). Interestingly, the powder spectrum slightly differs from the SDS thin film spectra at the spectral region around 1686 cm^{-1}, which can be attributed to C-O stretching vibrations.

It has to be noted here that no-contact imaging by using cassegrain objectives was not sensitive enough and contact microspectroscopic imaging by ATR would have the tendency to spread or remove the SDS thin films from the respective substrate surfaces. This is why we lay the focus here on μ-Raman imaging (so-called 'μ-Raman mapping') of SDS model contaminant films.

Typical Raman bands of the SDS can be easily observed in the spectra collected on Si and SST substrates, which are mainly characterized by the vibrational bands of the C-C skeleton at 1130 cm^{-1}, 1083 cm^{-1} and 1063 cm^{-1}, by the CH_2 twisting mode at 1296 cm^{-1}, by the bending vibrations of CH_2 groups around 1460 cm^{-1} and by the asymmetric and symmetric stretching vibrations of CH_x groups in the range 2800-3100 cm^{-1}. Specific vibrational signals of the SO_3 group can be mainly found in the Raman spectrum at 632 cm^{-1}, 597 cm^{-1}, 420 cm^{-1} together with a peak at 1083 cm^{-1} attributed to the $_{vs}SO_4$ that partially overlaps the above-mentioned C-C vibration. No specific signals related to the SST were found in the Raman spectrum of the bare substrate (data not shown), while typical Raman bands of Si were found in the region between 500-1500 cm^{-1} of the spectrum where the 1^{st}, 2^{nd} and 3^{rd} order at 520 cm^{-1}, 1000 cm^{-1} and 1450 cm^{-1} are shown, respectively. Absent or no-interfering overlapping of the Raman signals was observed on these two substrates, allowing an easy identification of the SDS fingerprint on the analyzed surfaces. Micro-Raman mapping was also exploited on these samples to analyze the distribution of the SDS on the surface at sub-micrometric scale. As the chemical images in Fig. 4a-b show, the SDS is not evenly distributed on the surface but small round-shaped convex protrusions of SDS aggregates occur on these substrates. This is due to the amphoteric nature of the SDS molecule which is arranged into micellar structures in polar solutions, by turning its polar headgroups towards the hydrophilic methanol , and its lipophilic tails inwardly towards the center of each micelle. When sprayed onto the different substrates, the micellar structures are maintained more or less in their original shapes.

Fig.4

The same analysis was also performed on the HDPE substrate. However, the detection of the SDS on the HDPE was not as straightforward as we observed in the previous cases. As the SDS on HDPE spectra of Fig.4c show, HDPE has very intense vibrational modes which tend

to overlap most of the SDS signals in the Raman spectrum. Raman signals of the HDPE are mainly present in the spectral region between 3000-2800 cm^{-1} and 1500-1300 cm^{-1} where the typical stretching and bending vibrations of the CH_x groups occur, respectively. The CH_2 wagging at 1297 cm^{-1} and the C-C stretching vibrations at 1131 and 1064 cm^{-1} are also shown. Two other small bands are present at 1370 and 1083 cm^{-1} which are assigned to the CH_3 wagging and to the C–C stretching, respectively, indicating the presence of an amorphous phase of the HDPE, while the bands at 1463 cm^{-1}, 1441 cm^{-1}, 1418 cm^{-1} and 1170 cm^{-1} are ascribed to the crystalline phase. These signals are clearly visible in all spectra in Fig.4c. In order to reveal the SDS on this substrate, a reference Raman spectrum of the bare HDPE (Fig.4c) was manually subtracted to the ones collected on different locations on the substrates, indicated as points from 1 to 4 in the optical image of Fig. 4d. In particular, as Fig. 4e shows, the presence of the SDS on the surface can be specifically revealed by the appearance of the overlapping modes of the C-C and SO_4 at 1083 cm^{-1} after the subtraction. Moreover, another typical mode of the SO_3 is also present at 597 cm^{-1} (data not shown), albeit weaker than the one at 1083 cm^{-1}. Therefore, micro-Raman characterization was demonstrated to be a valid tool for a non invasive and surface sensitive detection of SDS on all three different types of substrates used here, whilst also retaining information about the spatial distribution of the contaminant on the surface.

SDS contaminated real biomedical devices – Analyses on Hip Liners applying Ambient and Vacuum-based techniques

In the previous section we focused on the multi-technique characterization of SDS model contaminants with respect to chemical composition, identification and distribution across the different types of substrates by using elemental- and molecular-specific methods. However, in

industrial manufacturing, biomedical devices such as hip liners, for instance, do not possess any ideally flat or simple geometry, and impurities and contaminants may preferably settle down / stick to relatively inaccessible regions, with potential impact on quality control. The analytical tools discussed below that are commonly used for characterization of flat sample systems will be applied to a SDS-contaminated and non-contaminated polyethylene-based hip liner having a convex geometrical setting. SDS deposition was performed on the convex surface, i.e. outer part of the hip liner, using a concentration value of 0.25 mg/mL because it is close to the CMC of SDS. In reality, such a dosing level is likely to be well below an inhibitory concentration if present on an implant, owing to the large dilution factor encountered when the implant is placed in contact with body fluids during and after surgical implantation (many millilitres). In-vitro cultured cells may also be more susceptible to inhibition when chemically challenged, but 0.25 mg/mL was used because it provides a sufficiently challenging test concentration with regards to testing analytical detection capabilities.

Ambient mass spectrometry – analysis of hip liner

Having carried out preliminary testing of three AMS modalities the analysis of real world samples by DESI and LESA is required. A hip-liner of the kind used in modern hip replacement surgery was used for this purpose. A hip liner is employed to receive the ball of the femoral head, providing a lower friction surface for rotation of the joint as it sits within this new acetabular component within the recipients hip socket. The investigated hip liner was constructed from ultra-high-molecular-weight polyethylene (UHMWPE). The structure of UHMWPE is $(C_2H_4)_n$ with n greater than 100,000 and as such only the lower *m/z* multimer fragments of this polymer will have the potential to be detected in these experiments, in

addition to low mass contaminant compounds on its surface. The instrument configuration for sampling and transfer to the mass analyser differs for DESI and LESA [40–42]. Consequently, LESA, with its decoupled sampling and ionization steps and the differing requirements of sample surface position relative to the sampling probe and MS inlet, is potentially more amenable to analysis of more topographically challenging objects.

Fig.5

As a result, LESA MS was able to be carried out on both the convex and concave surfaces of the hip liner, whereas DESI MS was not able to sample successfully from the concave surface. Additionally, data obtained from the convex surface by DESI MS exhibited similar ion intensity but considerably larger variance than that from LESA MS (Fig. S-1 ESM).

Negative ion mode LESA spectra recorded from an untreated and SDS coated hip liner surface are shown in Figure 5a and b respectively. From the untreated hip liner surface, ions are detected in the range of m/z 519-602 with a mass difference of ± 56.06 Da indicating the presence of (C_4H_8)- groups characteristic of PE. After coating with an approximately 50 nm thick SDS film, the molecular anion $[M\text{-}Na]^-$ at m/z 265.14 was detected by LESA (Figure 5b), similar to that seen from SDS on flat PE (Figure 2). LESA was able to sample from the angled surface both on the inside (concave) and outside (convex) of the hip liner surface, Figure 5d-e respectively. In addition, during LESA analysis, MS/MS collision induced dissociation (CID) data were acquired from the peak at m/z 265.14, helping confirm the structural identity of the ion from its fragmentation pattern (Figure 5c).

FTIR and Raman micro-spectroscopical analyses

Both spectroscopic techniques were used for the SDS contaminant probing on a hip liner sample. Determination of whether ATR and contactless Raman analysis combined with a

microscopical setup serve as appropriate tools for chemical identification of nm layered SDS surface contaminant film spread over the convex side of a hip liner was investigated. The μ-Raman imaging permits spectra to be obtained from very small sample regions of interest, down to less than 1 μm laterally, and, likewise for FTIR, a few microns in depth in general. However, it has to be pointed out that Raman is a scattering technique which is more sensitive to sampling and optical design parameters, consequently small variations may lead to large effects on signal response and signal-to-noise ratios [43], especially in the case of non-ideally flat sample surfaces.

Fig.6

The ATR analysis on the convex hip liners shows that spectral contributions originating from SDS contamination (Table S-3) could be successfully detected on their surface (Fig. 6a). However, it has to be noted here that the CH stretching modes from the SDS do overlap with the HDPE modes in the 3100 - 2700 cm^{-1} spectral region. Clear spectral differences can be observed in the 1400 – 900 cm^{-1} spectral window that comprises mainly stretching modes from the SO_4 moieties of the SDS.

Micro-Raman point mapping was also performed on several locations on the external convex surface of the device demonstrating its applicability even on substrates with a complex geometry. An uncoated hip liner was measured as blank sample. As Fig.6b shows, Raman characterization of the outer hip liner surface suffers from the strong polyethylene background that overlaps with most of the SDS signals in the CH_x stretching and bending regions at 3000 - 2800 cm^{-1} and 1500 – 1000 cm^{-1}, respectively. However, specific signals of the SDS can be observed at 632 cm^{-1}, 597 cm^{-1} and 420 cm^{-1} attributed to the vibrations of the SO_3 moieties and in the peak at 1083 cm^{-1} which is interpreted as an overlapping of the SO_4 and C-C skeletal vibration of the molecule.

The SDS contaminant signal is neither hindered nor altered, albeit slight signal intensity variations could be detected for both vibrational spectroscopic techniques, hence, a distinct identification on samples having a complex geometry is feasible by using both complementary Raman and IR spectroscopies.

XRF for absolute SDS quantification on Hip Liners

In addition to the flat model systems, real medical devices were analyzed. A hip liner with a non-flat shape represents a challenging measurement geometry for GIXRF due to the curved surface. In particular for the grazing incidence regime the angle of incidence is difficult to determine and consequently also the solid angle of detection. To prevent this, a calibrated aperture is used to provide a well-defined solid angle of detection.

The hip liners were analyzed using a photon energy of about 1487 eV to excite all the relevant elements excluding sulfur. The incidence angle is here of about 10°. For the analysis of the hip liners blanks were available and were analyzed as well. The measurements showed small Na contaminations which are significantly smaller, approximately one order of magnitude of the fraction of SDS. Here, a subtraction of the Na background is possible and was carried out. The GIXRF spectra exhibit further contaminations of small amounts of N, Fe, and Mg. These contaminants are also observable on the coated hip liners.

In Table 2, the experimentally determined mass deposition of O and Na is shown for the uncoated and coated samples. On basis of the Na content and the knowledge of the stoichiometry, the mass deposition of C, H, S, and O has been determined. Hence, the thickness of the SDS layer is calculated assuming the bulk density of SDS. The SDS contaminated hip liners were analyzed at two different positions, the center and two millimeters away from the center. The thickness at the center position is about 50 nm, which

is the same as the target value of the spray coating. But the value of the off-center measurement is considerable smaller, less than 40% of the expected value.

Table 2

The analysis of contaminants on curved surfaces is feasible but with an increased experimental effort in particular in grazing incidence geometry, which is necessary for the quantitative characterization of small amounts of contaminants. This elaborative reference-free approach is paid off as it lays the foundation for the traceable determination of certain contaminations regarding elemental composition and content, in view of developing new reference materials for organic compounds that are scarcely available.

Conclusions

In this systematic inter-comparative approach, we showed and discussed the characterization of deliberately deposited SDS films mimicking contaminations on inorganic and organic substrates, potentially used as reference materials for ambient techniques, i.e. Ambient mass spectrometries, Raman and Infrared spectroscopy, to reliably determine amounts of contamination.

Our results demonstrated that the complementary information provided by non-invasive vibrational spectroscopies can be gathered qualitatively, thus increasing reliability in identification of even thin film contaminant layers by their unique Raman and IR spectral fingerprints in the presence of diverse bulk substrate settings. IR and Raman readout tools evidenced the existence of contaminants, even on an emulated SDS-contaminated real biomedical device, i.e. a hip liner with a convex / concave sample geometry. Both techniques may help for reliably and quickly identifying surface impurities during or after industrial processing and can be combined with chemical imaging to reliably localize the SDS

contamination on the µm scale. Both readout techniques may be slotted in ahead of the other remaining techniques discussed in our approach, followed by the traceable reference-free XRF analysis. This technique allowed quantification of the Na content originating from the SDS, both on model SDS contaminant layer systems and on the convex side of a hip liner. Specifically, the mass deposition of C, Na, and O was absolutely determined, leading to a dtermined layer thickness of 50 nm on the hip liner, thus, being in line with the intended applied SDS contamination to the real biomedical device.

As with Raman and FTIR spectroscopies, AMS provided fingerprint outputs for a fast qualitative identification of surface contaminations. AMS should be used at the end of the traceability chain since it is a moderately destructive technique relying on the removal of material from the sample surface to provide measurements. However, these techniques may even be able to elucidate the state of polymerization, and consequently the resulting extent of polymeric surface cleanliness. For the complex hip liner geometry and large sample size LESA enabled more flexibility in sampling, and gave better signal repeatability for the detection of SDS. Further work towards quantitative measurements from real world samples would significantly benefit the utility of these AMS data for industrial applications.

The increase of information depth provided by combining all techniques has the potential to enable even on-line characterization and chemical speciation within the process chain in the biomedical device industry.

Acknowledgements and Funding Information

We acknowledge financial support by the European Metrology Research Programme (EMRP). This work was funded through the EMRP Project IND56 Q-AIMDS. The EMRP is

jointly funded by the EMRP participating countries within EURAMET and the European Union.

We would like also to acknowledge Jean-Luc Vorng for the technical support on AMS results interpretation.

Compliance with ethical standards

Conflict of Interest: The authors declare that they have no conflict of interest.

Research involving Human Participants and/or Animals: not applicable.

Informed consent: not applicable.

References

1. Andrascik K. K-Andrascik. In: Kanegsberg BK and E, editor. Handbook for Critical Cleaning. 2nd Applic. CRC Press; 2011. p. 574.
2. Albert DE. D-Albert. Developments in Surface Contamination and Cleaning. William Andrew Applied Science Publishers; 2015. p. 109–28.
3. Li L. Overview of MS and MALDI MS for polymer analysis. MALDI mass spectrometry for synthetic polymer analysis. Hoboken: John Wiley & Sons, Inc.; 2009. p. 1–9.
4. Chen HW, Talaty NN, Takats Z, Cooks RG. Desorption electrospray ionization mass spectrometry for high-throughput analysis of pharmaceutical samples in the ambient environment. Anal Chem. 2005 Nov;77(21):6915–27.
5. Griffiths RL, Randall EC, Race AM, Bunch J, Cooper HJ. Raster-Mode Continuous-Flow Liquid Microjunction Mass Spectrometry Imaging of Proteins in Thin Tissue Sections. Anal Chem. 2017;89(11):5683–7.
6. Ferreira CR, Yannell KE, Jarmusch AK, Pirro V, Ouyang Z, Cooks RG. Ambient Ionization Mass Spectrometry for Point-of-Care Diagnostics and Other Clinical Measurements. Clin Chem. 2016 Jan;62(1):99 LP-110.
7. Pollakowski-Herrmann B, Hornemann A, Giovannozzi AM, Green F, Gunning P, Portesi C, et al. Journal of Pharmaceutical and Biomedical Analysis A calibration procedure for a traceable contamination analysis on medical devices by combined X-ray spectrometry and ambient spectroscopic techniques. J Pharm Biomed Anal. Elsevier B.V.; 2018;150:308–17.
8. Tuchin V V, Chiou A, Heinemann S. Part One Process Control and Quality Assurance.

In: Popp J, Tuchin V V., Chiou A, Heinemann and S, editors. Handbook of Biophotonics Photonics in Pharmaceutics, Bioanalysis and Environmental Research. 1st ed. Wiley-VCH Verlag GmbH & Co. KGaA; 2012. p. 1–70.

9. Patel R, Patel KS. Flow injection determination of anionic surfactants with cationic dyes in water bodies of central India. Analyst. 1998;123(8):1691–5.

10. Sakai T, Harada H, Liu XQ, Ura N, Takeyoshi K, Sugimoto K. New phase separator for extraction-spectrophotometric determination of anionic surfactants with Malachite Green by flow injection analysis. Talanta. 1998;45(3):543–8.

11. Chan WH, Lee AWM, Lu JZ. Optode for the specific determination of anionic surfactants. Anal Chim Acta. 1998 Mar;361(1–2):55–61.

12. Sharvelle S, Lattyak R, Banks MK. Evaluation of biodegradability and biodegradation kinetics for anionic, nonionic, and amphoteric surfactants. WATER AIR SOIL Pollut. 2007;183(1–4):177–86.

13. Rosen MJ, Li F, Morrall SW, Versteeg DJ. The relationship between the interfacial properties of surfactants and their toxicity to aquatic organisms. Environ Sci Technol. 2001 Mar;35(5):954–9.

14. Pojjak K, Meszaros R. Novel Self-Assemblies of Oppositely Charged Polyelectrolytes and Surfactants in the Presence of Neutral Polymer. LANGMUIR. 2009;25(23):13336–9.

15. Rodenas-Torralba E, Reis BF, Morales-Rubio A, de la Guardia M. An environmentally friendly multicommutated alternative to the reference method for anionic surfactant determination in water. Talanta. 2005 Apr;66(3):591–9.

16. Arand M, Friedberg T, Oesch F. Calorimetric Quantitation of Trace Amounts of Sodium Lauryl Sulfate in the Presence of Nucleic Acids and Proteins. Anal Biochem. 1992;207:73–5.

17. Zheng C-L, Ji Z-X, Zhang J, Ding S-N. A fluorescent sensor to detect sodium dodecyl sulfate based on the glutathione-stabilized gold nanoclusters/poly diallyldimethylammonium chloride system. Analyst. 2014;139(13):3476–80.

18. Fu W, Qu F, Yu G, You J. High selectivity for sodium dodecyl sulphate by polymer nanoparticles and detection of proteins based on the polymer nanoparticles-sodium dodecyl sulphate system. SENSORS AND ACTUATORS B-CHEMICAL. 2017;245:774–9.

19. Hao X, Lei JL, Li NB, Luo HQ. An electrochemical sensor for sodium dodecyl sulfate detection based on anion exchange using eosin Y/polyethyleneimine modified electrode. Anal Chim Acta. 2014;852:63–8.

20. Inacio AS, Mesquita KA, Baptista M, Ramalho-Santos J, Vaz WLC, Vieira O V. In Vitro Surfactant Structure-Toxicity Relationships: Implications for Surfactant Use in Sexually Transmitted Infection Prophylaxis and Contraception. PLoS One. 2011;6(5).

21. Senf F, Flechsig U, Eggenstein F, Gudat W, Klein R, Rabus H, et al. A plane-grating monochromator beamline for the PTB undulators at BESSY II. J Synchrotron Rad. 1998;5:780–2.

22. Scholze F, Beckhoff B, Brandt G, Fliegauf R, Klein R, Meyer B, et al. New PTB beamlines for high-accuracy EUV reflectometry at BESSY II. Proc SPIE. 2000. p. 72.

23. Beckhoff B, Ulm G. Determination of fluorescence yield using monochromatized undulator radiation of high spectral purity and well-known flux. Adv X-Ray Anal. 2001;44:349–54.

24. Lubeck J, Beckhoff B, Fliegauf R, Holfelder I, Hönicke P, Müller M, et al. A novel instrument for quantitative nanoanalytics involving complementary X-ray methodologies. Rev Sci Instrum [Internet]. 2013;84(4). Available from: http://scitation.aip.org/content/aip/journal/rsi/84/4/10.1063/1.4798299

25. Beckhoff B, Fliegauf R, Kolbe M, Müller M, Weser J, Ulm G. Reference-Free Total Reflection X-ray Fluorescence Analysis of Semiconductor Surfaces with Synchrotron Radiation. Anal Chem. American Chemical Society; 2007;79(20):7873–82.

26. Ratcliffe L V, Rutten FJM, Barrett DA, Whitmore T, Seymour D, Greenwood C, et al. Surface analysis under ambient conditions using plasma-assisted desorption/ionization mass spectrometry. Anal Chem [Internet]. American Chemical Society; 2007 Aug 15 [cited 2016 Aug 18];79(16):6094–101. Available from: http://pubs.acs.org/doi/abs/10.1021/ac070109q#.V7VgvhKqT3M.mendeley

27. Wiseman JM, Laughlin BC. Desorption Electrospray Ionization (DESI) Mass Spectrometry: A brief introduction and overview. Current Separations and Drug Development. p. 11–4.

28. Randall EC, Race AM, Cooper HJ, Bunch J. MALDI Imaging of Liquid Extraction Surface Analysis Sampled Tissue. Anal Chem. 2016;88(17):8433–40.

29. Salter TL, Green FM, Faruqui N, Gilmore IS. Analysis of personal care products on model skin surfaces using DESI and PADI ambient mass spectrometry. Analyst. 2011;44(0):3274–80.

30. Feikes J, Von Hartrott M, Ries M, Schmid P, Wüstefeld G, Hoehl A, et al. Metrology Light Source: The first electron storage ring optimized for generating coherent THz radiation. Phys Rev Spec Top - Accel Beams. 2011;14:030705-1-030705-10.

31. Wüstefeld RM and AH and AM and AS and GU and JF and MR and G. Status of the IR and THz beamlines at the Metrology Light Source. J Phys Conf Ser. 2012;359(1):12004.

32. Nefliu M, Venter A, Cooks RG. Desorption electrospray ionization and electrosonic spray ionization for solid- and solution-phase analysis of industrial polymers. Chem Commun. 2006;(8):888–90.

33. Salter TL, Gilmore IS, Bowfield A, Olabanji OT, Bradley JW. Ambient Surface Mass Spectrometry Using Plasma-Assisted Desorption Ionization: Effects and Optimization of Analytical Parameters for Signal Intensities of Molecules and Polymers. Anal Chem. 2013 Feb;85(3):1675–82.

34. Calligaris D, Caragacianu D, Liu X, Norton I, Thompson CJ, Richardson AL, et al. Application of desorption electrospray ionization mass spectrometry imaging in breast cancer margin analysis. Proc Natl Acad Sci U S A. 2014;111(42):15184–9.

35. Nielen MWF, Hooijerink H, Zomer P, Mol JGJ. Desorption electrospray ionization mass spectrometry in the analysis of chemical food contaminants in food. TRAC-TRENDS Anal Chem. 2011 Feb;30(2, SI):165–80.

36. Bowfield A, Bunch J, Salter TL, Steven RT, Gilmore IS, Barrett DA, et al.

Characterisation of a micro-plasma for ambient mass spectrometry imaging. Analyst. 2014;139(21):5430–8.

37. Kim JY, Seo ES, Kim H, Park J-W, Lim D-K, Moon DW. Atmospheric pressure mass spectrometric imaging of live hippocampal tissue slices with subcellular spatial resolution. Nat Commun. 2017;8.

38. Salter TLR, Bunch J, Gilmore IS. Importance of Sample Form and Surface Temperature for Analysis by Ambient Plasma Mass Spectrometry (PADI). Anal Chem. 2014;86(18):9264–70.

39. Krimm S, Liang CY, Sutherland GBBM. Infrared Spectra of High Polymers. II. Polyethylene*. J Chem Phys. 1956;25(3):549–62.

40. Wu C, Dill AL, Eberlin LS, Cooks RG, Ifa DR. Mass spectrometry imaging under ambient conditions. MASS Spectrom Rev. 2013;32(3):218–43.

41. Kocurek KI, Stones L, Bunch J, May RC, Cooper HJ. Top-Down LESA Mass Spectrometry Protein Analysis of Gram-Positive and Gram-Negative Bacteria. J Am Soc MASS Spectrom. 2017;28(10):2066–77.

42. Kocurek KI, Griffiths RL, Cooper HJ. Ambient ionisation mass spectrometry for in situ analysis of intact proteins. J MASS Spectrom. 2018;53(7):565–78.

43. McCreery RL. Raman Spectroscopy for Chemical Analysis. John Wiley & Sons, Inc.; 2005.

Figure Legends

Fig. 1 - XRF spectra of the SDS model contaminant films prepared on different substrates. Spectra were recorded at 1622 eV.

Fig. 2 Negative ion mode was applied for acquisition of (a) DESI mass spectra and (b) LESA mass spectra of a 50 nm thick SDS film on HDPE substrate, measured in the mass range from 200 m/z – 500 m/z. The dashed line indicates the SDS molecule anion.

Fig. 3 (a) FTIR spectra of SDS layers on Si, SST and HDPE and (b) corresponding Raman data. The FTIR and Raman spectra of pure SDS are displayed here as reference in the upper part of the graph (a) and (b), respectively.

Fig. 4 Micro Raman images of SDS layers on Si (a) and SST (b). Raman spectra of SDS layers on HDPE at different locations on the substrate (c). The correspondent locations are shown in the optical image in figure (d). Normal and Raman difference spectra (after the subtraction of the HDPE reference) correspond to the locations indicated by the points from 1 to 4 in the spectral region between 1150-1070 cm^{-1} (e).

Fig. 5 - Negative ion mode LESA mass spectra of a polyethylene hip liner for (a) an untreated surface with the PE peaks marked with circles, (b) the SDS coated surface with the anion of SDS, m/z 265.147 marked with a star for the mass range m/z 100 to 800, and (c) the MS/MS of the m/z 265.147 peak showing the fragmentation of the sulphate and the hydrocarbon. Image of LESA sampling of the concave inner surface of a hip liner (d) and the convex, outer surface of a hip liner (e).

Fig. 6 FTIR (a) and Raman (b) spectral averages calculated from nine different locations single spectra onto the hip liner surface (poly-ethylene) without any SDS coating (top) and of the SDS-coated hip-liner (bottom), respectively.

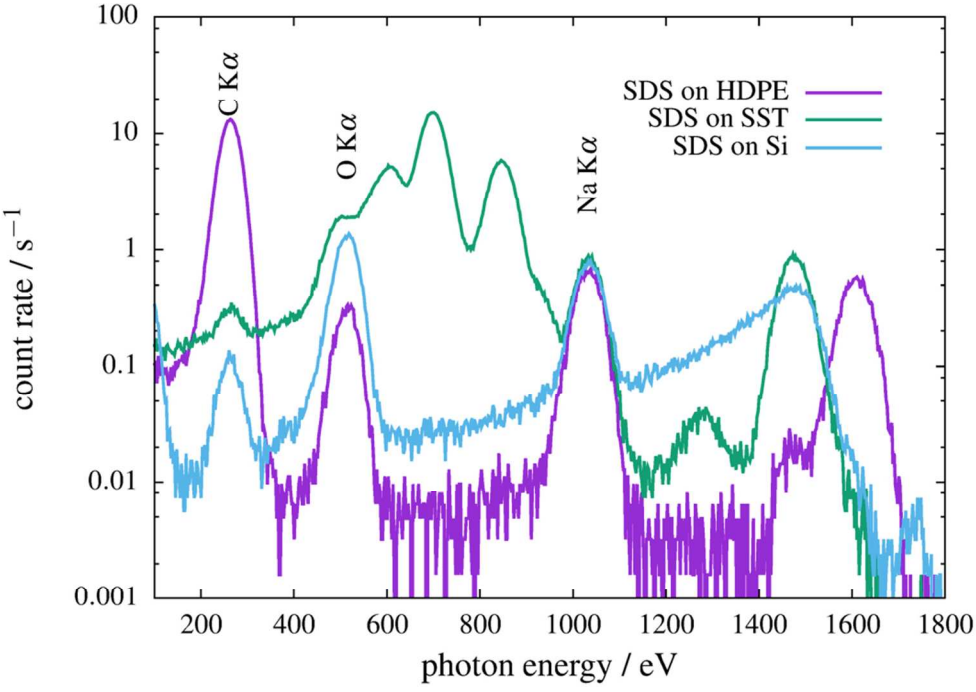

Fig. 1 - XRF spectra of the SDS model contaminant films prepared on different substrates. Spectra were recorded at 1622 eV.

125x86mm (220 x 220 DPI)

Table 1 Measurements at 1622 eV for the quantification of Na, C, and O.

Mass deposition* / ×10^{-7} g/cm^2					**Uncertainties**	**15% (k=1)**
Sample	Carbon	Oxygen	Sodium			
SDS on SST	13 ± 2	25 ± 4	3.5 ± 0.5			
SDS on HDPE	n.a.	9.2 ± 1.4	3.3 ± 0.5			
SDS on Si	17 ± 3	36 ± 5	2.9 ± 0.4			
Mass deposition* / ×10^{-7} g/cm^2						
Sample	Carbon	Oxygen	Sodium	Sulfur	Hydrogen	Thickness / nm
SDS on SST	22	9.8	3.5	4.9	3.8	44 ± 6
SDS on HDPE	20	9.1	3.3	4.6	3.6	41 ± 6
SDS on Si	18	8.2	2.9	4.1	3.2	37 ± 6

*Mass deposition data (calculated arithmetic means) derived from five single measurements, respectively. The second part shows the calculated mass deposition based on the sodium content assuming stoichiometric SDS and its concluded thickness.

161x134mm (150 x 150 DPI)

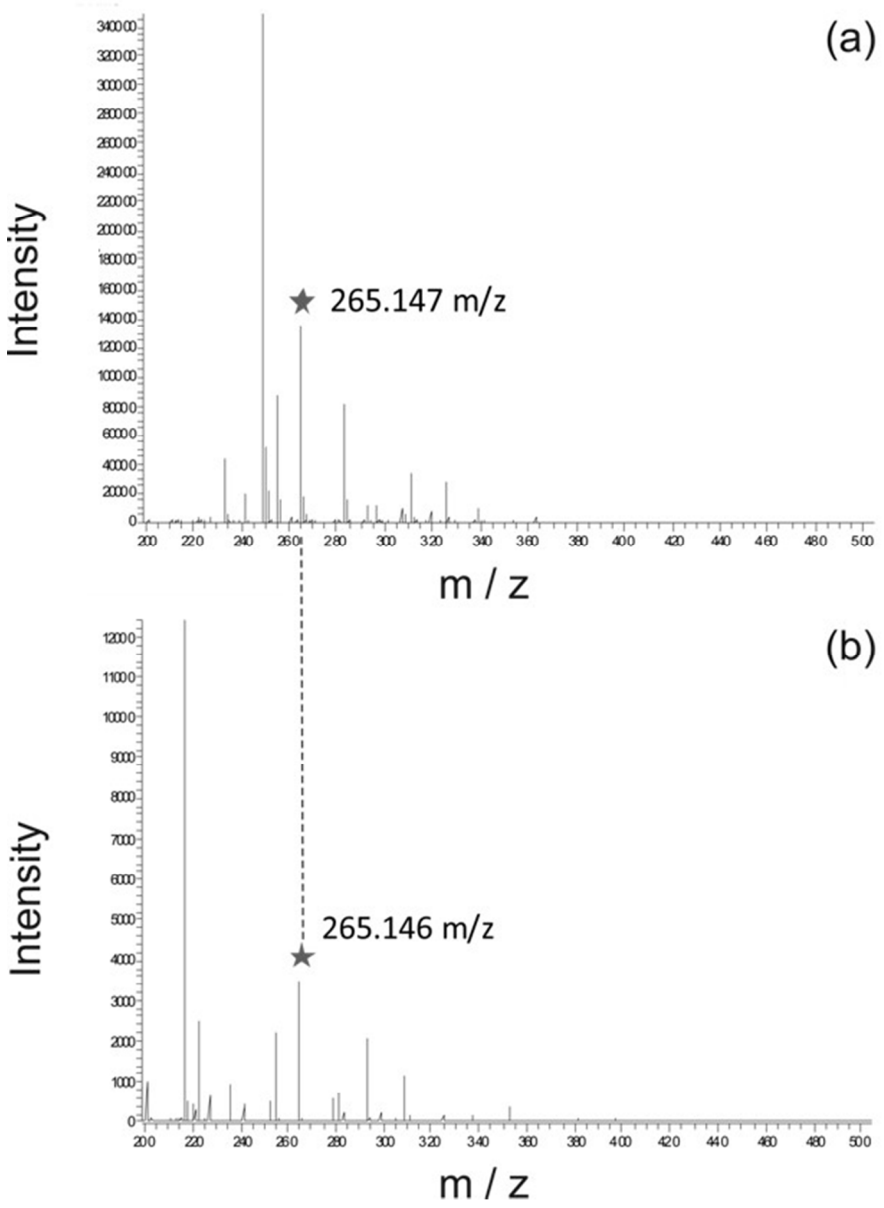

Fig. 2 Negative ion mode was applied for acquisition of (a) DESI mass spectra and (b) LESA mass spectra of a 50 nm thick SDS film on HDPE substrate, measured in the mass range from 200 m/z – 500 m/z. The dashed line indicates the SDS molecule anion.

105x141mm (150 x 150 DPI)

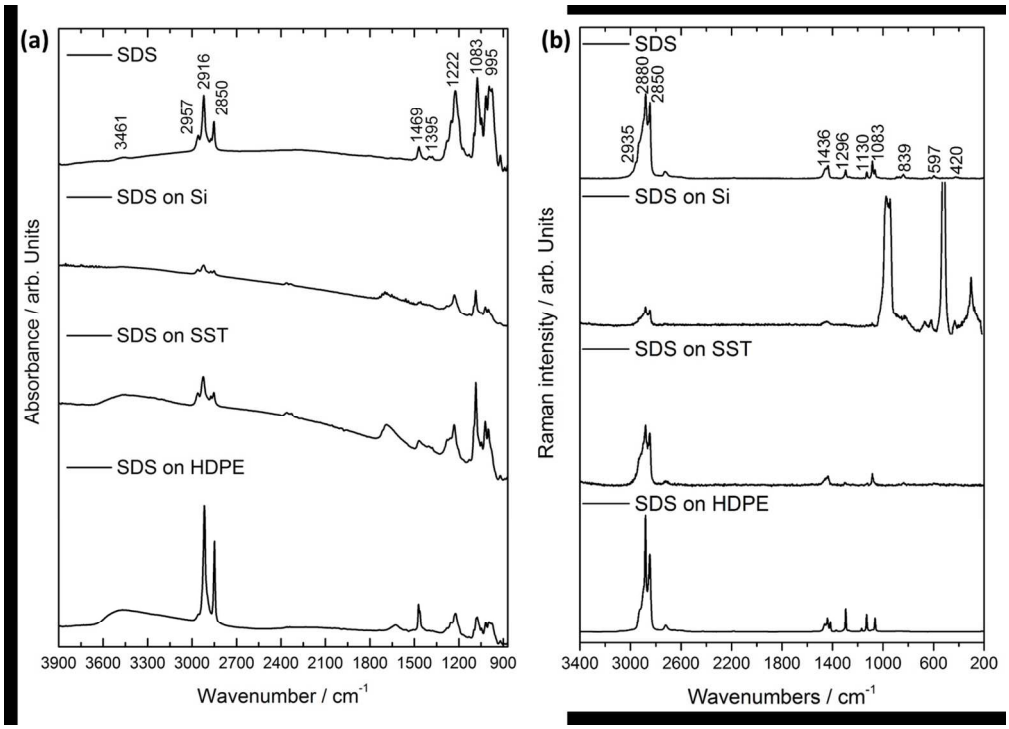

Fig. 3 (a) FTIR spectra of SDS layers on Si, SST and HDPE and (b) corresponding Raman data. The FTIR and Raman spectra of pure SDS are displayed here as reference in the upper part of the graph (a) and (b), respectively.

246x177mm (150 x 150 DPI)

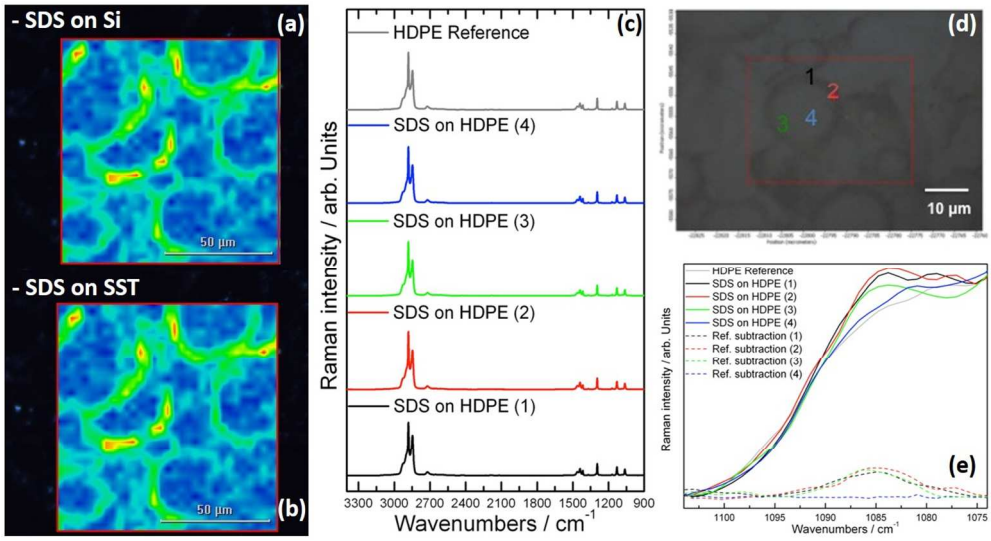

Fig. 4 Micro Raman images of SDS layers on Si (a) and SST (b). Raman spectra of SDS layers on HDPE at different locations on the substrate (c). The correspondent locations are shown in the optical image in figure (d). Normal and Raman difference spectra (after the subtraction of the HDPE reference) correspond to the locations indicated by the points from 1 to 4 in the spectral region between 1150-1070 cm^{-1} (e).

252x136mm (150 x 150 DPI)

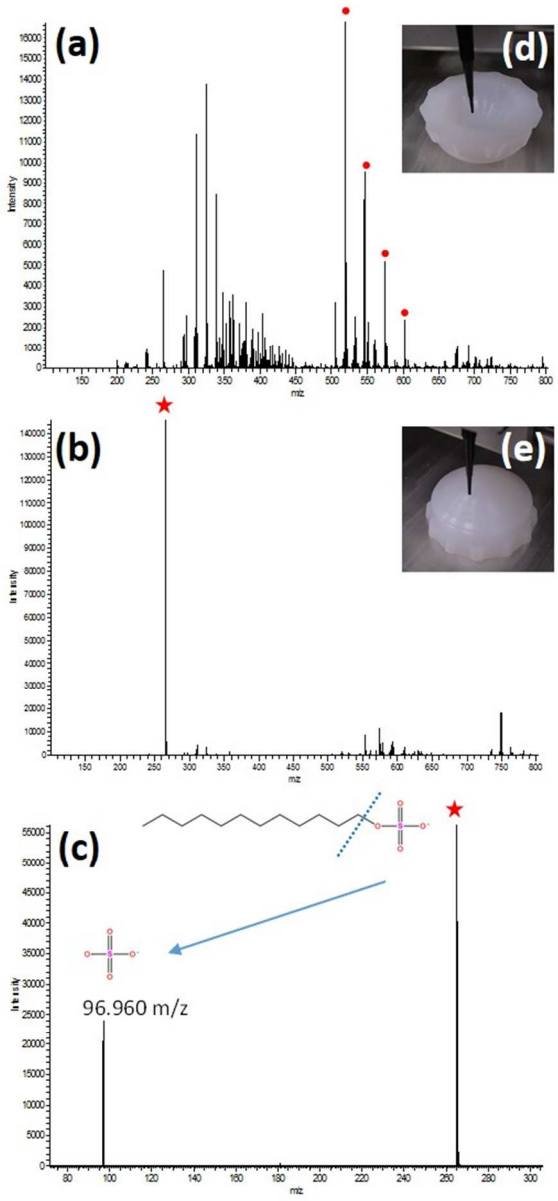

Fig. 5 - Negative ion mode LESA mass spectra of a polyethylene hip liner for (a) an untreated surface with the PE peaks marked with circles, (b) the SDS coated surface with the anion of SDS, m/z 265.147 marked with a star for the mass range m/z 100 to 800, and (c) the MS/MS of the m/z 265.147 peak showing the fragmentation of the sulphate and the hydrocarbon. Image of LESA sampling of the concave inner surface of a hip liner (d) and the convex, outer surface of a hip liner (e).

88x184mm (150 x 150 DPI)

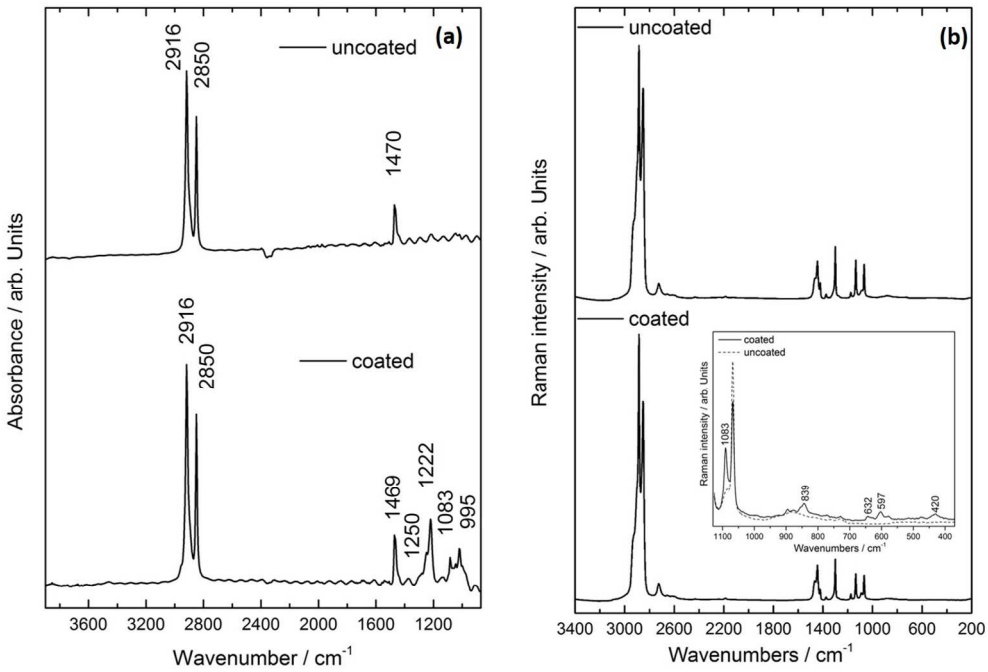

Fig. 6 FTIR (a) and Raman (b) spectral averages calculated from nine different locations single spectra onto the hip liner surface (poly-ethylene) without any SDS coating (top) and of the SDS-coated hip-liner (bottom), respectively.

254x175mm (150 x 150 DPI)

Table 2 Measurements at 1487 eV for the quantification of Na and O.

Mass deposition / $\times 10^{-7}$ g/cm²					**Uncertainties**	**15% (k=1)**
Sample	Carbon	Oxygen	Sodium			
Off-center	n.a.	7.38	1.910			
Center	n.a.	13.8	4.530			
'Reference'	n.a.	348	0.510			
Mass deposition / $\times 10^{-7}$ g/cm²						
Sample	Carbon	Oxygen	Sodium	Sulfur	Hydrogen	Thickness / nm
Off-center	8.77	3.90	1.40	1.95	1.52	18
Center	25.1	11.2	4.02	5.59	4.37	50

169x106mm (150 x 150 DPI)

Electronic Supplementary Material (ESM)

A methodological inter-comparison study on the detection of surface contaminant sodium dodecyl sulfate applying ambient- and vacuum-based techniques

Andrea M. Giovannozzi[a,*], Andrea Hornemann[b], Beatrix Pollakowski-Herrmann[b], Felicia Green[c], Paul Gunning[d], Tara L. Salter[e], Rory T. Steven[c], Josephine Bunch[c,f], Chiara Portesi[a], Bonnie Tyler[g], Burkhard Beckhoff[b], and Andrea M. Rossi[a]

[a]*Quality of Life Division, INRIM, Strada delle Cacce 91, 10135 Torino, Italy*

[b]*Physikalisch-Technische Bundesanstalt Berlin (PTB), Abbestr. 2-12, 10587 Berlin, Germany*

[c]*National Centre of Excellence in Mass Spectrometry Imaging (NiCE-MSI), National Physical Laboratory, TW11 0LW, United Kingdom*

[d]*Smith & Nephew Research Centre, York Science Park, Heslington, York, YO10 5DF, United Kingdom*

[e]*Department of Chemistry, School of Life Sciences, University of Sussex, Falmer, Brighton, BN1 9QJ, UK*

[f]*Department of Surgery & Cancer, Computational and Systems Medicine, Imperial College London, SW7 2AZ, UK*

[g]*University of Münster, 48149 Münster, Germany*

[*]*Corresponding author:*

Dr. Andrea M. Giovannozzi,

tel +39 011 3919330

fax +39 011 346384

e-mail a.giovannozzi@inrim.it

Further theoretical details on ***Reference-free XRF***

The quantitative analysis of the absolute mass per unit area and the elemental composition is carried out by using a fundamental parameter approach as introduced in Beckhoff et al. [1]. Here, all experimental and atomic fundamental parameters have to be well-known. For this purpose, the calibrated instrumentation is used. The atomic fundamental parameters are taken from databases, e.g. Elam database [2]. Excluding the photoelectric cross section it follows from the Ebel database [3] and the fluorescence yield for the carbon K edge follows from [4] according to the equation:

$$\frac{m_i}{F_I} = \frac{-1}{\mu_{tot,i}} \ln\left\{1 - \frac{P_i}{P_{0,Wsurf}\,\tau_{i,E_0}\,Q\,\frac{\Omega_{det}}{4\pi}\,\frac{1}{\sin\psi_{in}}\,\frac{1}{\mu_{tot,i}}}\right\}$$

Table S-1 Parameters for the equation given above with their tentative assignments and meanings.

Parameter	Tentative assignments
E_0	photon energy of the incident (excitation) radiation
$P0 = S_0/\sigma_{Diode,E0}$	radiant power of the incident radiation
S_0	signal of the photodiode measuring the incident radiation
$\sigma_{Diode,E0}$	spectral responsitivity of the photodiode
Ψ_{in}	angle of incidence with respect to the wafer surface
E_i	photon energy of the fluorescence line *l* of the element *i*
Ψ_{out}	angle of observation
R_i	detected count rate of the fluorescence line *l* of the element *i*
$\varepsilon_{Det,Ei}$	detection efficiency of the SDD detector at the photon energy E_i
Ω_{Det}	effective solid angle of detection
$\mu_{i,E}$	absorption cross section of the element *i* at the photon energy *E*

	$\mu_{tot,i} = \mu_{i,E_0} / \sin\psi_{in} + \mu_{i,E_i} / \sin\psi_{out}$
τ_i	photo electric cross section of the element *i* at the photon energy
G	transition probability of the fluorescence line *l* belonging to *Xi*
Ω	fluorescence yield of the absorption edge *Xi*
Q	$Q = \omega_{Xi}\, g_{l,Xi}$

Further details on **Results & Discussion**

Ambient Mass spectrometry – PADI, DESI and LESA

Table S-2 Detection of SDS from HDPE, SS and Si using DESI for 50 nm thick films using both 50:50 MeOH:H_2O and 90:10 ACN:H_2O.

Sample	Ion intensity of molecular anion [$C_{12}H_{25}O_4S^-$ at m/z 265.147] (number of molecular ions × 10^6)	
SDS thickness (Solvent used)	50 nm (MeOH:H_2O)	50 nm (ACN:H_2O)
SDS on SST	1.86 ± 0.21	0.15 ± 0.03
SDS on HDPE	2.32 ± 0.73	9.56 ± 0.73
SDS on Si	6.62 ± 2.28	0.26 ± 0.08

FTIR and Raman (micro-) spectroscopical analyses

The detection of SDS coating was successful, characteristic and mutually complementary Raman and IR fingerprints could be detected. Modes and their tentative assignments are listed in Table S-3.

Table S-3 Raman and mid-infrared vibrational modes of sodium dodecyl sulfate (SDS). ν: stretching, δ: deformation. as, s: (a)symmetrical. τ: twisting. ρ: rocking

Raman Modes / cm^{-1}	Assignments [5] /cm^{-1}	Infrared Modes/ cm^{-1}	Assignments [6–8]
420	SO_3	n.a.	n.a.
597	SO_3	n.a.	n.a.
632	SO_3	n.a.	n.a.
839	S-OC	n.a.	n.a.
891	ρ CH_2	n.a.	n.a.
n.a.	n.a.	995	ν C-C
n.a.	n.a.	1021	$\nu_s (OSO_3^-)$
1063	ν_{asym} C-C trans	n.a.	n.a.
1083	$\nu_s SO_4$ /ν C-C gauche	1083	$\nu_s (OSO_3^-)$
1130	ν_{sym} C-C trans	n.a.	n.a.
n.a.	n.a.	1222	$\nu_{as} (OSO_3^-)$
n.a.	n.a.	1250	$\nu_{as} (OSO_3^-)$
1295	τ CH_2	n.a.	n.a.
1435	δ CH_2	n.a.	n.a.
1455	δ CH_2	1469	δ CH_2
2846	ν_{sym} CH_2	2850	ν_{sym} CH_2

2860	ν_{sym} CH_3 Fermi res.	n.a.	n.a.
2880	ν_{asym} CH_2	2916	ν_{as} CH_2
2900	Fermi resonance	n.a.	n.a.
2935	Fermi resonance	n.a.	n.a.
2961	ν_{asym} CH_3	2957	ν_{as} CH_3

Ambient Mass spectrometry – hip liner

The comparison of LESA and DESI MS on the convex region of the hip liner was carried out on two hip liners where one was deliberately contaminated and one analysed as-received. These analyses were carried out in triplicate and the results are shown in Figure S-1 below.

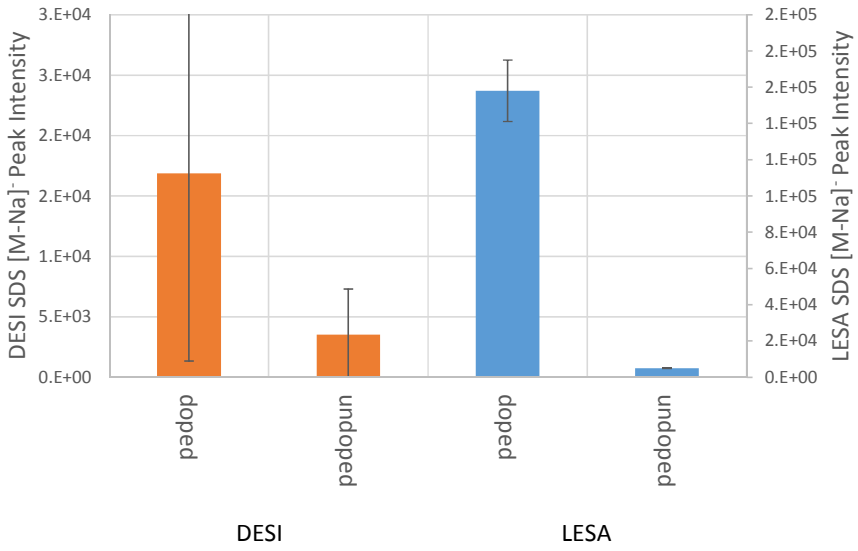

Figure S-1 - Mean signal intensities for SDS $[M\text{-}Na]^-$, *m/z* 265.147, from the hip liner surface with and without SDS doping for DESI and LESA.

The detection of SDS on the as-received samples was low but non-zero for LESA and with higher but more variable signal via DESI with the consequence that these data are not significantly different statistically. The detected ion intensity for the doped surface hip liner has a similar

relationship with respect to spread of data with LESA being notably less variable than DESI and with an apparent substantial difference in ion intensity that is consequently not statistically significant. Therefore, these data suggest similar results from both DESI and LESA MS analysis of doped and un-doped surfaces and supports the applicability of these techniques for in-line industrial analysis. However, the larger variability and stricter sampling geometry requirements mark LESA MS the more appropriate technique DESI in this particular example.

References

1. Beckhoff B, Fliegauf R, Kolbe M, Müller M, Weser J, Ulm G. Reference-Free Total Reflection X-ray Fluorescence Analysis of Semiconductor Surfaces with Synchrotron Radiation. Anal Chem. American Chemical Society; 2007;79(20):7873–82.
2. Elam WT, Ravel BD, Sieber JR. A new atomic database for X-ray spectroscopic calculations. Rad Phys Chem. 2002;63:121–8.
3. Ebel H, Svagera R, Ebel MF, Shaltout A, Hubbell JH. Numerical description of photoelectric absorption coefficients for fundamental parameter programs. X-Ray Spectrom. 2003;32(6):442–51.
4. Beckhoff B, Ulm G. Determination of fluorescence yields using monochromized undulator radiation of high spectral purity and well known flux. Adv X-Ray Anal. 2001;44:349–54.
5. PICQUART M. VIBRATIONAL-MODE BEHAVIOR OF SDS AQUEOUS-SOLUTIONS STUDIED BY RAMAN-SCATTERING. J Phys Chem. 1986;90(2):243–50.
6. Viana RB, da Silva ABF, Pimentel AS. Adsorption of Sodium Dodecyl Sulfate on Ge Substrate: The Effect of a Low-Polarity Solvent. Int J Mol Sci. Molecular Diversity Preservation International (MDPI); 2012 Jun 28;13(7):7980–93.
7. Urban MW, König JL. Spectroscopic Studies of Interactions between Styrene-Acrylic Acid Copolymer and Sodium Dodecyl Sulfate. 1987. p. 1028–32.
8. Gao X, Chorover J. Adsorption of sodium dodecyl sulfate (SDS) at ZnSe and a -Fe 2 O 3 surfaces : Combining infrared spectroscopy and batch uptake studies. J Colloid Interface Sci. Elsevier Inc.; 2010;348(1):167–76.